Structure, Vol. 10, 1581–1592, November, 2002, ©2002 Elsevier Science Ltd. All rights reserved. PII S0969-2126(02)00882-1

Structural and Biochemical Analysis of the Obg GTP Binding Protein

John Buglino, Vincent Shen, Payam Hakimian, and Christopher D. Lima[1]
Biochemistry Department
Structural Biology Program
Weill Medical College of Cornell University
New York, New York 10021

Summary

The Obg nucleotide binding protein family has been implicated in stress response, chromosome partitioning, replication initiation, mycelium development, and sporulation. Obg proteins are among a large group of GTP binding proteins conserved from bacteria to man. Members of the family contain two equally and highly conserved domains, a C-terminal GTP binding domain and an N-terminal glycine-rich domain. Structural analysis of *Bacillus subtilis* Obg revealed respective domain architectures and how they are coupled through the putative switch elements of the C-terminal GTPase domain in apo and nucleotide-bound configurations. Biochemical analysis of bacterial and human Obg proteins combined with the structural observation of the ppGpp nucleotide within the Obg active sight suggest a potential role for ppGpp modulation of Obg function in *B. subtilis*.

Introduction

GTP binding proteins are conserved throughout life and are widely used as binary switches for cellular processes that include signal transduction, protein translocation, trafficking, and cell cycle control [1]. Families of GTP binding proteins are widely varied and include heterotrimeric GTP binding proteins, small Ras-like GTP binding proteins, and translation-elongation GTP binding factors. GTP binding proteins generally transduce signals to downstream effectors by altering their conformations in response to GTP binding. Subsequent γ-phosphate hydrolysis and GDP exchange resets the switch for activation [2]. A hallmark of most GTP binding proteins is a slow intrinsic rate of GTP hydrolysis and the inability to quickly exchange GDP for GTP in the absence of exogenous exchange factors. In many Ras-like GTPases, the duration of the activated state, GTP hydrolysis, and GDP exchange are aided or inhibited by the action of three factors, GAFs (guanine activating factors), GEFs (guanine exchange factors), and GDIs (guanine dissociation inhibitors) [3].

Although GTP binding proteins have enjoyed widespread study over the years, several highly conserved GTP binding protein families coupled to domains of unknown function have only recently been uncovered by successful completion of numerous genome sequences [4–6]. The Obg family of GTP binding proteins belongs to this group (Figure 1). Although the exact biochemical function for Obg has remained elusive, Obg has been extensively characterized in several bacteria that undergo complex transitions, such as sporulation and differentiation. *Bacillus subtilis* Obg (BsObg) is a 428-amino acid protein that contains the conserved N-terminal glycine-rich domain (1–158), the GTP binding domain (159–342), and an additional C-terminal TGS domain (343–428). The TGS domain has no known function, but it is named for three protein families in which it is found, *T*hrRS, *G*TPase, and *S*poT [7]. TGS is a small domain consisting of approximately 50 amino acids that has been suggested to encode a nucleotide binding role.

BsObg was first identified as a cotranscribed element within the Spo0B operon, functionally implicating BsObg in the Spo0A phosphorelay system that regulates the onset of sporulation through Spo0A transcription factor activation [8]. Evidence supporting this function was uncovered in screens for sporulation defects through use of a temperature-sensitive allele and conditional expression, revealing that *obg* is essential for vegetative growth and efficient sporulation [9–11]. BsObg was purified and shown to bind and hydrolyze GTP and readily exchange GDP for GTP [10, 12]. Rapid GDP-GTP exchange in the absence of exogenous exchange factors led to the hypothesis that *Bacillus subtilis* Obg could control sporulation by directly sensing GTP/GDP ratios in the cell. The model predicts that, under optimal growth conditions, GTP-BsObg suppresses sporulation and that, upon experiencing starvation or stress conditions, GTP levels diminish and force the equilibrium toward GDP-BsObg. Other functional models for BsObg have arisen, suggesting direct interaction with the ribosome and a role in stress activation of σ^B through interaction with the Rsb proteins [13, 14]. Overproduction of Obg, gene replacement, and analysis of Ras-like mutations within consensus Obg GTP binding motifs in *Streptomyces coelicolor* and *Streptomyces griseus* indicate that the nucleotide-bound state of Obg controls formation of aerial mycelium and morphological differentiation without effecting vegetative growth [15, 16].

The *Caulobacter crescentus* Obg protein is encoded by *cgtA* and is essential for cell growth [17]. Detailed biochemical analysis of the CgtA protein revealed guanine nucleotide specificity, GTP and GDP affinities, GTP hydrolysis rates, and GDP-GTP exchange properties [18]. The overall rate constants measured for CgtA agree well with those obtained for the *B. subtilis* Obg protein, showing slow rates for hydrolysis (0.03 min^{-1}), micromolar binding constants for both GDP and GTP, and rapid dissociation constants for either GTP or GDP ($\sim$1.5 s^{-1}). These data, if interpreted in the absence of potential GAPs, GEFs, or GDIs, suggest the nucleotide-bound state of Obg would be controlled by relative GTP/GDP concentrations, consistent with a role for Obg in sensing and transducing signals based on the nutritional envi-

[1]Correspondence: lima@pinky.med.cornell.edu

Key words: G protein; GTPase; ppGpp; Ras; Obg; signal transduction

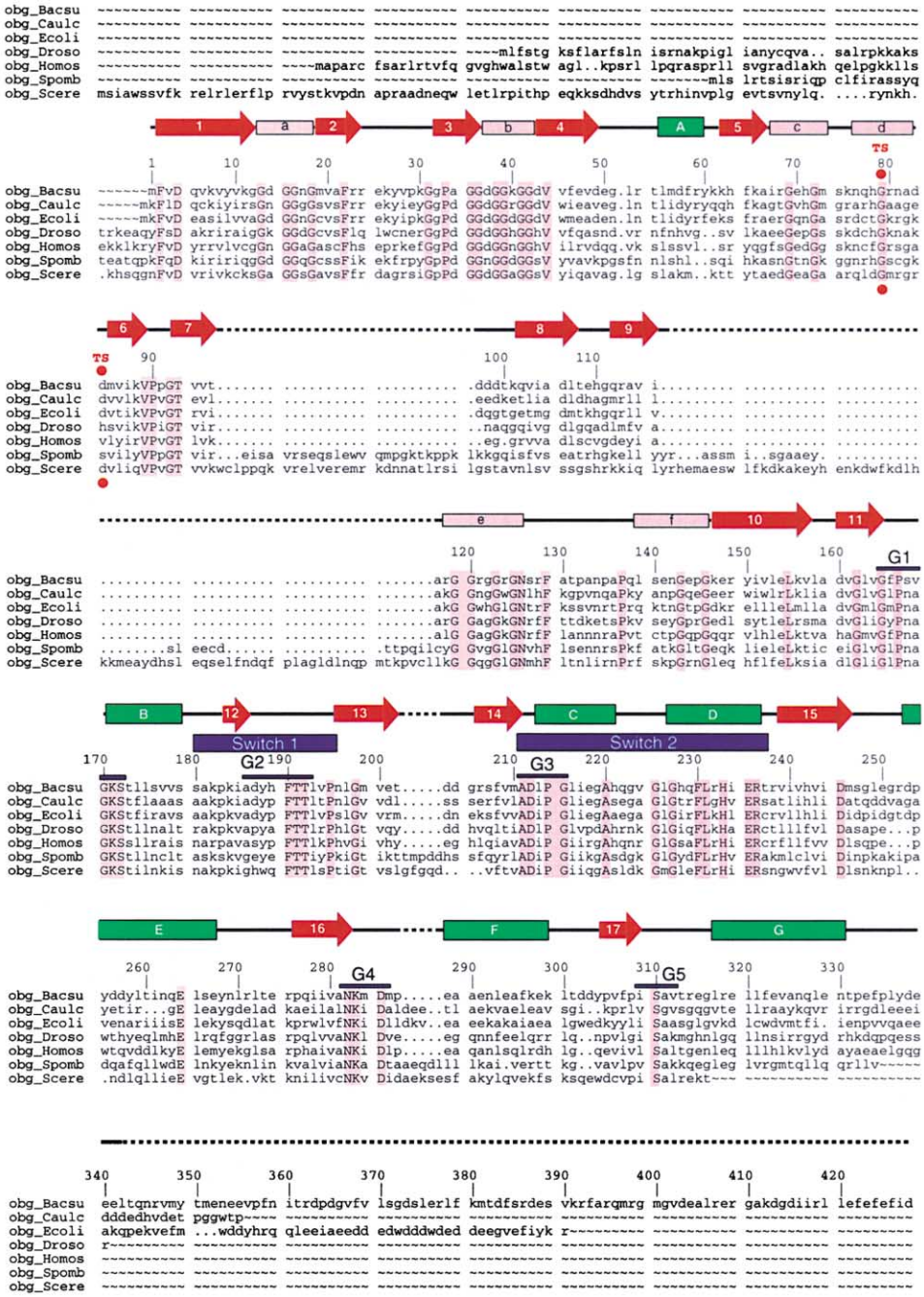

Figure 1. Structure-Based Sequence Alignment for Obg Family Members

Sequences include *B. subtilis* Obg (obg_Bacsu) and other Obg orthologs from *C. crescentus* (obg_Caulc), *E. coli* (obg_Ecoli), *D. melanogaster* (obg_Droso), *H. sapiens* (obg_Homos), *S. pombe* (obg_Spomb), and *S. cerevisiae* (obg_Scere). Gaps are denoted by dots. Numbering is done with respect to full-length BsObg. The secondary structure for BsObg is shown above the sequence, with β strands numbered (red), helices lettered (green), type II helices lettered (lower case in pink bars), and coils depicted as lines. Side chain identity is shown in pink-highlighted capital letters. Conserved G protein elements are shown as G1–G5 over dark lines, and switch elements are denoted by dark blue bars over the sequence. Temperature-sensitive alleles isolated in *E. coli* and *B. subtilis* are denoted by red circles above and below the respective sites.

ronment in the cell. The CgtA N-terminal glycine-rich domain was shown not to function as a GEF [19], and mutational analysis of putative GTPase switch 1 residues that diminish GTP binding activity were shown to be essential in vivo, linking Obg nucleotide specificity to in vivo function [20].

More recent studies in *E. coli* have revealed *obgE* as an essential gene and that expression of the *E. coli* Obg protein (EcObg) is required for cellular growth [21]. A temperature-sensitive *obgE* allele, conditional expression, and overexpression all suggested that ObgE was required for replication-independent chromosomal par-

titioning, resulting in elongated cells that do not divide. Similar phenotypes were uncovered in *Vibrio harveyi* with a *cgtA* insertional mutant, although these studies described additional defects in DNA replication synchronization [22]. Biochemical analysis of *E. coli* Obg revealed a monomeric enzyme with similar enzymatic properties to those reported for other bacterial Obg proteins with regard to nucleotide binding and hydrolysis (see above). Unlike BsObg, EcObg did not comigrate with ribosomes, but cofractionated with bacterial membranes in an EDTA-dependent manner. Gel retardation assays further revealed EcObg DNA binding activity, although no specific element within EcObg was directly implicated in this activity.

While several potential Obg functions have been uncovered in bacteria, no coherent function or biochemical activity has been assigned to the Obg protein family. Furthermore, little effort has been focused on eukaryotic Obg function. To address the poorly understood function for Obg and other highly conserved and large-molecular weight GTP binding proteins, we have initiated a structural biology program focused on the elucidation and characterization of their three-dimensional structures and biochemical properties. Our first effort in this program included characterization of the Obg protein to uncover the basis for Obg catalytic activity and to reveal the architecture for the unique glycine-rich N-terminal domain. To this end, we have determined the 2.6 Å resolution X-ray structure for conserved elements within the Obg protein family and have made attempts to characterize elements within Obg to assay respective catalytic and binding activities for bacterial and human Obg proteins.

Results and Discussion

Bacillus subtilis Obg contains three domains, a conserved N-terminal domain (1–158) that does not share structural, functional, or sequence similarity to any other known protein, a conserved GTP binding domain (161–342) that shares overall fold topology with the small Ras-like GTPases, and a C-terminal TGS domain (~342–428) not widely conserved between Obg family members, but shared between bacterial stress response proteins, such as SpoT [7, 23] (Figure 1). Limited proteolysis led to the identification of a BsObg fragment that included residues 1 to ~342 [Obg(1–342)p], a fragment that displayed wild-type GTPase activity and included the N-terminal glycine-rich domain and the Ras-like GTPase domain, the two elements conserved between all Obg family members (Figures 1 and 2; see Experimental Procedures).

Selenomethionine-substituted protein [24] produced diffraction-quality crystals that were used to obtain phases for Obg(1–342)p by multiwavelength anomalous diffraction [25] at Advanced Photon Source beamline 19-ID. The structure was refined to 2.6 Å, to an R factor of 0.204 and an R_{free} of 0.293, and included two BsObg molecules in the asymmetric unit. One monomer was observed in a nucleotide-bound state and includes 328 amino acid residues (1–185 and 195–337). The other monomer was observed in its apo state and included 342 amino acids (1–342) (see Experimental Procedures and Table 1). The Obg and GTP binding domains are organized end to end and are autonomous, in that neither domain exchanges its polypeptide chain into the other domain. The interface between domains is large and mediated, in part, by the conserved putative GTPase switch elements, suggesting potential nucleotide-dependent interactions and feedback between the two domains (see below). Analysis of the molecule reveals an elongated structure that measures over 100 Å in one dimension (Cα to Cα). The overall dimensions for the N-terminal Obg domain and nucleotide binding domain are 10 × 5 × 70 Å and 45 × 35 × 30 Å, respectively (Cα to Cα).

Structure and Composition of the Glycine-Rich Domain

The N-terminal Obg domain appears unique (Figures 1 and 2), since no sequence similarity can be observed between this domain and other protein sequences in the database. Additionally, no structural similarities were observed between this domain and other domains in the Protein Data Bank, as computed by DALI [26]. Because of its unique attributes, we will refer to this domain as the "Obg fold" throughout the text. The Obg fold (residues 1–158 in the *B. subtilis* protein) is found in all known Obg nucleotide binding proteins. The *B. subtilis* Obg fold contains 26 glycine residues organized into linear sequence motifs, 21 of which are conserved between family members (Figure 1). The structure determination of the Obg N-terminal domain elucidated three major features, the structure and organization of the glycine-rich sequence motifs, the structure of the polypeptide between glycine-rich motifs that protrudes from the tip of the Obg fold, and the organization of the interface between the base of the Obg fold and the putative switch elements of the C-terminal GTPase domain (Figures 2 and 3).

Structural analysis revealed that the glycine-rich motifs comprise six left-handed type II helices that share structural similarity to a canonical type II polyproline helix. Each type II helix is denoted by italicized lower case letters throughout the text (*a*, *b*, *c*, *d*, *e*, and *f*). The helices are observed in pairs (*a*-*b*, *c*-*d*, and *e*-*f*) and pack together in both parallel and antiparallel fashion (Figures 2 and 3). Each pair is arranged above and below the other, such that the *a*-*b* pair is packed between the *c*-*d* pair and the *e*-*f* pair. The helices arrange to form a complex main chain hydrogen bonding pattern, with each helix making at least one main chain hydrogen bonding interaction with at least two other helices (Figure 3). Sequence analysis and amino acid conservation does not reveal the repeating type II structural elements observed within the Obg domain. Although each type II helix is approximately seven amino acids long, each helical sequence motif is unique. The two central helices (*a*-*b*) contain the highest glycine content, a feature that is likely required for optimal packing and hydrogen bonding interactions between helices *c*-*d* and *e*-*f* (Figure 3). The glycine-rich helices form a structure that does not contain a standard hydrophobic core as is observed in most proteins. The fold appears to gain specificity

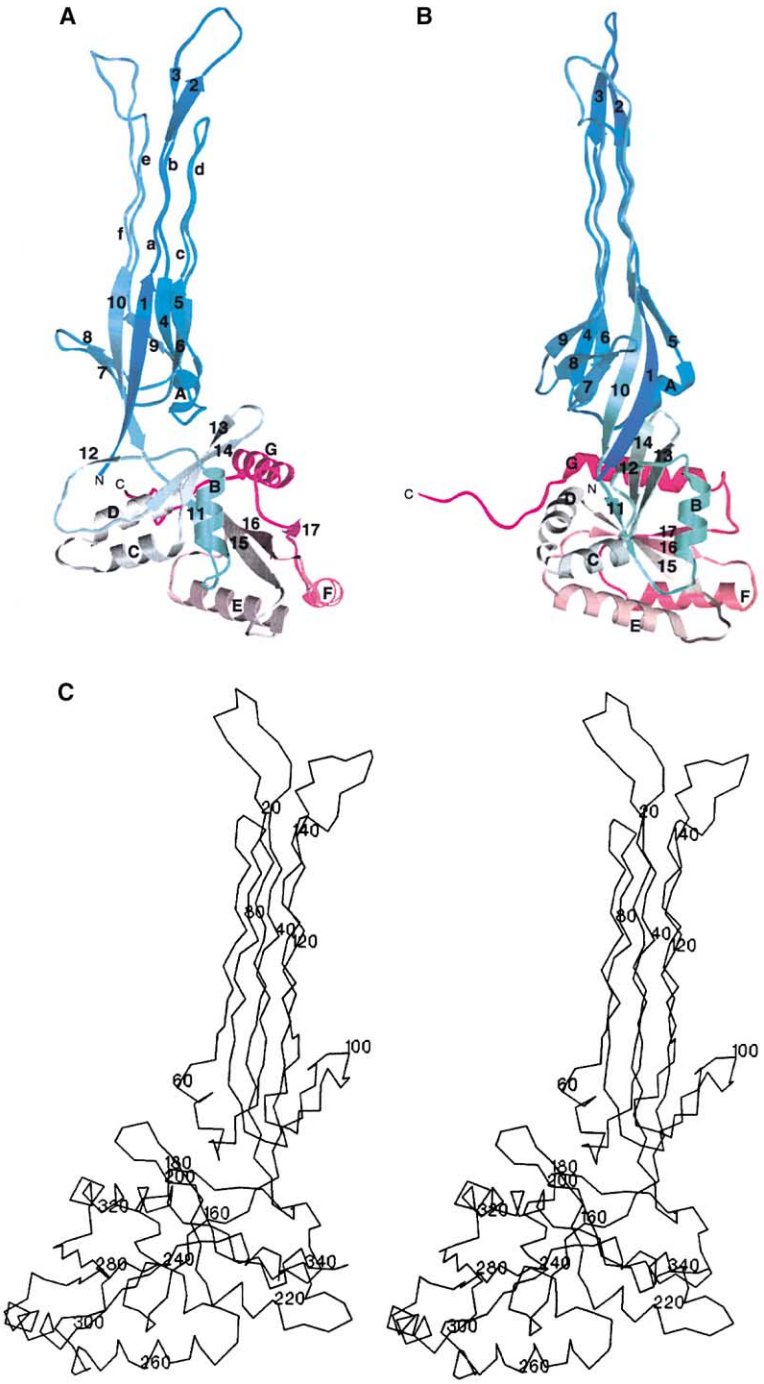

Figure 2. Structure of the Obg Protein

(A and B) Orthogonal ribbon diagrams of the Obg protein. β strands are numbered, α helices are lettered, and type-II helices are lettered in lowercase italics in (A). N- and C-terminal residues are denoted in capital italics. Color-coding from blue to red of the main chain ribbon is from the N terminus to the C terminus.

(C) Stereo representation of the Obg protein, with Cα positions numbered every 20 residues. Graphics were prepared with SETOR, unless otherwise noted [43].

through a series of side chain-mediated salt-bridging interactions and side chain to main chain hydrogen bonding interactions emanating from the surface of the fold (Figure 3C). Sequence conservation is low between amino acids on the surface, suggesting that structural conservation of the Obg fold is more important than conservation of individual residues on the Obg fold surface (Figure 4).

The second segment of the Obg fold includes residues between each of the type II helices, the length of which is conserved between Obg family members (Figures 1 and 2). The loops between helices *a*-*b* and *e*-*f* are extensive compared with the loop between *c*-*d*. Comparison between both Obg monomers in the asymmetric unit revealed the conformation of these loops to be largely similar, although conformational flexibility was observed for amino acids 24–29 in the largest loop between *a*-*b* helices. The length of residues in these intervening segments is conserved from bacteria to man, suggesting that these residues play an important functional role in Obg. Conservation of loop length between helical pairs is in direct contrast to other regions within the Obg fold

Table 1. Crystallographic Data

Resolution (Å)	Wavelength (Å)	Reflections (unique/total)	Coverage (%)	(I/σ)	R_{sym}[a]
25–2.6	1.0163 (preedge)	39,920/74,532	86.1 (68.0)	9.3 (2.3)	0.075 (0.36)
25–2.6	0.9796 (edge)	39,571/72,293	84.3 (62.1)	8.0 (2.2)	0.081 (0.37)
25–2.6	0.9794 (peak)	38,652/70,639	82.5 (46.5)	8.4 (2.3)	0.079 (0.32)
25–2.6	0.9466 (remote)	38,758/70,402	83.8 (62.7)	7.7 (3.1)	0.084 (0.38)

Anomalous Diffraction Ratios[b] (25–2.6 Å)

	Preedge	Edge	Peak	Remote
Preedge	0.055 (0.157)	0.071 (0.156)	0.071 (0.155)	0.059 (0.157)
Edge		0.079 (0.172)	0.054 (0.138)	0.074 (0.159)
Peak			0.100 (0.207)	0.070 (0.166)
Remote				0.073 (0.150)

Wavelength (25–2.6 Å)	R_{cullis}[c]		Phasing Power[d]	
	Centric Isomorphous	Acentric Isomorphous/ Anomalous	Centric Isomorphous	Acentric Isomorphous/ Anomalous
Preedge	—	—	—	—/0.46
Edge	0.49	0.53/0.83	2.19	2.51/1.79
Peak	0.53	0.56/0.78	2.13	2.21/1.89
Remote	0.68	0.68/0.92	2.64	2.00/1.32

FOM[e] (2.5–2.6 Å)

Acentric	0.53
Centric	0.55

Refinement	25–2.6 Å
Number of reflections greater than 0.0 σ	24,465 (99.4% complete)
Nonhydrogen atoms	
Protein	5,082
Water	484
Mg ions	7
Nucleotide	36
R_{cryst}[f]	0.204
R_{free}[g]	0.293
Rms deviations[h]	
Bond length (Å)	0.012
Bond angles (°)	1.36
B value main chain/side chain (Å^2)	1.50/1.94

All numbers in parentheses indicate last outer shell statistics.
[a] $R_{sym} = \Sigma|I - \langle I\rangle|/\Sigma I$, where I is the observed intensity and $\langle I\rangle$ is the average intensity.
[b] Anomalous diffraction ratios = $\langle\Delta|F|^2\rangle^{1/2}/|F|^2\rangle^{1/2}$, where $\Delta|F|$ is the absolute value of the Bijvöet (diagonal elements) or dispersive difference (off-diagonal elements), respectively.
[c] $R_{cullis} = \Sigma||Fh(obs)| - |Fh(calc)||/\Sigma|Fh(obs)|$ for centric reflections, where |Fh(obs)| is the observed heavy atom structure factor amplitude and |Fh(calc)| is the calculated heavy-atom structure factor amplitude.
[d] Phasing power = rms(|Fh|/E), where |Fh| is the heavy-atom structure factor amplitude and E is the residual lack of closure error.
[e] Figure of merit = $|F(hkl)_{best}|/F(hkl)$.
[f] R_{cryst}, R based on 95% of the data used in refinement.
[g] R_{free}, R based on 5% of the data withheld for the crossvalidation test.
[h] Rms deviations, root-mean-square deviations from ideal geometry and B factors for bonded atoms.

that includes insertions between α helix A and β strand 5 and large insertions between β strands 7 and 8 and between β strand 9 and type II helix *e*, all of which occur at the base of the Obg domain near the interface with the GTP binding domain (Figures 1 and 2).

The third segment of the Obg fold includes β strands 1 and 4–10 and α helix A. This segment provides a platform for the glycine-rich elements on one side and serves as the primary interface between the Obg fold and the GTP binding domain on the opposite side. Residues in the Obg fold that contact the GTP binding domain include amino acids at the N-terminal end of β strand 1, the loop between β strand 4 and α helix A, and residues at the C-terminal end of β strand 10. Although the only covalent association between the Obg fold and the GTP binding domain occurs between β strands 10 and 11, the interaction between domains is extensive, burying approximately 2690 Å^2 of accessible surface area between domains [27].

Data supporting an important functional role for the Obg fold arose from the isolation of temperature-sensitive *obg* alleles in *B. subtilis* and *E. coli* [9, 21]. In these studies, mutations that disrupt Obg function include G79E and D84N, two residues within the N-terminal glycine-rich domain, indicating that integrity of the Obg fold is required for in vivo function. Gly79 is conserved between Obg family members, and analysis of the structure suggests that Gly79 is critical to formation and stabilization of the Obg type II helical bundle through Gly79 backbone amide hydrogen bonding interactions

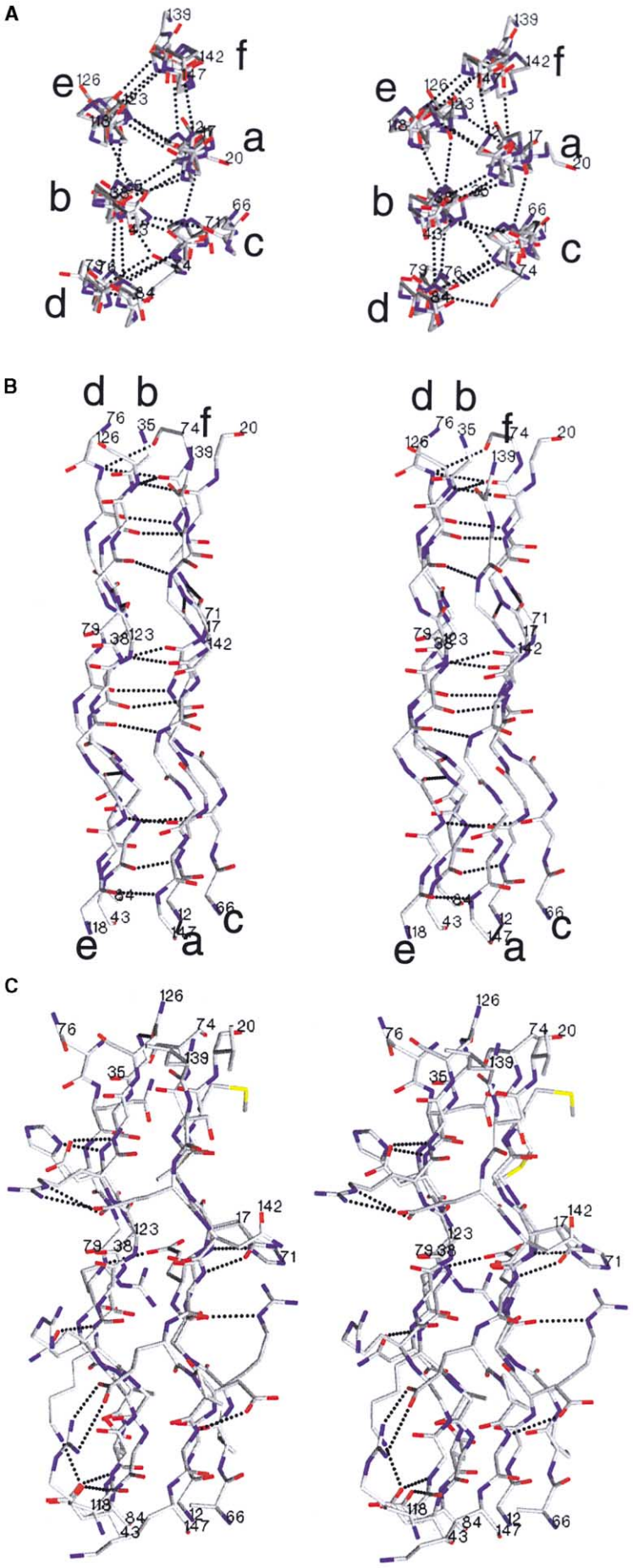

Figure 3. Structure of the Obg Glycine-Rich Domain

(A) Orthogonal stick diagram of the Obg glycine-rich domain, labeled as in Figure 2. View of the domain looking down the type II helical axis to accentuate the hydrogen bonding network formed between type II helices. Hydrogen bonds are shown as black dashed lines, and side chains were removed for clarity.

(B) Orthogonal view of the Obg glycine-rich domain as in (A).

(C) Orthogonal view of the Obg glycine-rich domain as in (B), with previous main chain hydrogen bonds deleted, side chains shown, and side chain to side chain or side chain to main chain hydrogen bonding interactions depicted by black spheres. Lower case letters are used to demarcate the N termini of each respective type II helix in (B).

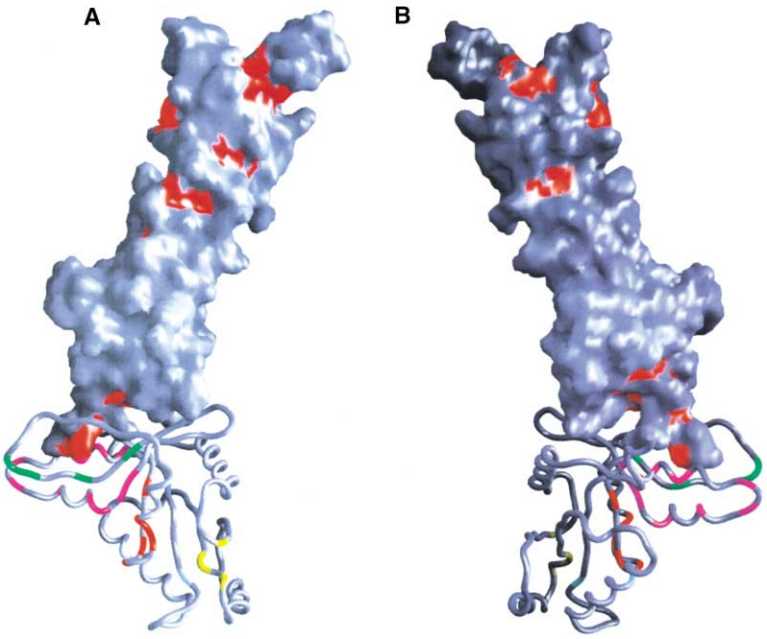

Figure 4. Surface View and Consensus Motifs for the Obg Protein

(A and B) A surface rendering is shown for the Obg domain (residues 1–158), and a worm representation is shown for the GTP binding domain (residues 159–342). Amino acid conservation between Obg family members is shown by red patches on the surface of the Obg domain (see Figure 1). Amino acid sequence identity in the GTP binding domain is shown by colors on the worm representation: red, conserved G1 residues; green, G2-switch 1 residues; magenta, G3-switch 2 residues; light-blue, residues 245 and 264; yellow, conserved G4–G5 residues. The N-terminal residues from the Obg fold (1–4) can be seen protruding into the cleft between the switch 1 and switch 2 regions. The figure was prepared with GRASP [27].

with the backbone carbonyl oxygen from Asp37. Although Asp84 makes side chain hydrogen bonding interactions with the backbone amide of Asp43, this residue is not conserved between family members, and the *ts* D84N substitution is conservative. As such, we surmise that G79E is the dominant mutation responsible for the *ts* phenotype, although the secondary D84N mutation could further weaken helix *d*, destabilizing the Obg fold at nonpermissive temperatures.

The architecture of the Obg glycine-rich domain was conceptually reminiscent of structural proteins such as collagen [28]. To address a platform or scaffolding role for the Obg domain, we undertook studies in bacteria and human systems to reveal interactions with binding partners, through direct biochemical fractionation, through yeast two-hybrid interactions, or through cellular localization. Although these experiments failed to produce interactions deemed relevant for Obg function in organisms where Obg is conserved, a BsObg N-terminal (1–161) fragment fused to glutathione S-transferase facilitated identification of a single protein obtained from pull-downs with *Bacillus subtilis* lysate (see Experimental Procedures). This experiment revealed a near 1:1 interaction between the glycine-rich domain (1–161) and a 30 kDa protein from *B. subtilis*. Sufficient quantities of the complex could be isolated, facilitating the identification of the Obg fold binding partner as CotN or TasA (SwissProt P54507).

TasA is a 30 kDa protein that is secreted into the medium early in sporulation and also incorporated into the endospore [29–31]. Although secreted, sporulating cultures of *B. subtilis* contain TasA in both intracellular and supernatant fractions, consistent with possible Obg-TasA interactions in the cell. We were unable to replicate these interactions in pull-downs using recombinant TasA produced from *E. coli*, suggesting that additional lysate-derived cofactors could be required for the interaction. TasA is regulated at the onset of sporulation by Spo0A, a transcription factor and phosphorelay system potentially regulated by Obg at the onset of sporulation [8]. TasA does not have any known orthologs in eukaryotes or other bacteria, indicating that Obg-TasA interaction would not be conserved in other organisms that contain Obg. Sequence analysis of Obg family members reveal distinctly conserved elements within members that are not shared across all known Obg proteins, indicating that the conserved Obg fold could be utilized in various pathways that are not conserved between all organisms that contain Obg. Utilizing clones of human Obg, we conducted subcellular localization in NIH-3T3 cells and a yeast two-hybrid Cyto-trap screen (Stratagene) to uncover genetic interactions between unknown protein effectors (see Experimental Procedures). These studies failed to produce interactions deemed relevant to a ubiquitous Obg function.

The Obg Active Site and Putative GTPase Switch Elements

The C-terminal GTP binding domain reveals sequence and structural similarity with other GTPase domains in the Protein Data Bank, as computed by DALI [26]. Several top-scoring structural matches in descending order include Arf, EF-TU, Ras, EF-G, Ran, Gi-α-1, and Era (see Experimental Procedures for Protein Data Bank codes, amino acid overlap, and sequence identities). The GTPase superfamily consensus motifs (G1–G5) are evident in the Obg GTP binding domain, although the putative Obg switch elements are divergent in sequence and length from those observed for the most closely related structural neighbors (Figure 1). On the basis of analogy to other GTPases, amino acids 180–195, located between helix B and β strand 13, would comprise the putative Obg switch 1 element. The putative switch 2 element is comprised of amino acids 211–237 and includes α helices C and D. Other nucleotide-dependent conformational changes in G5 were observed between

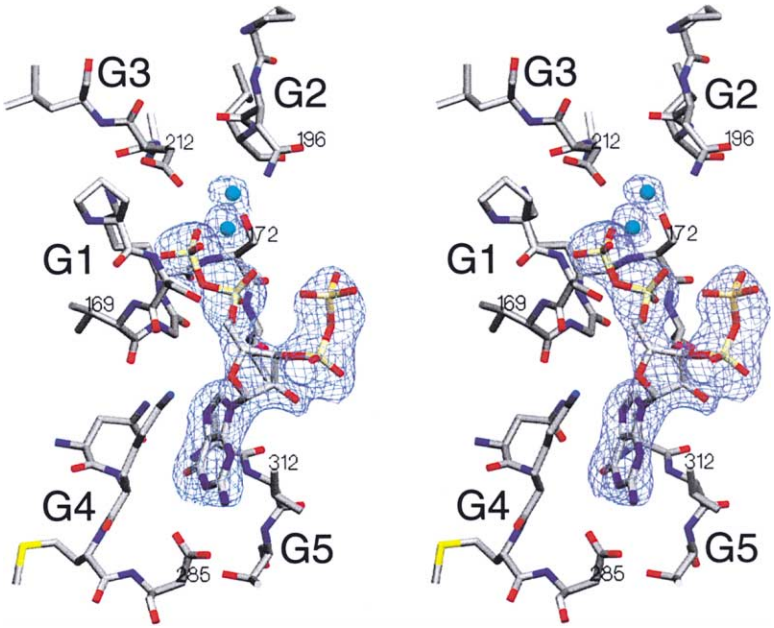

Figure 5. The Active Site and Bound Nucleotide

(A) Stereo representation of the active site, including residues from G1, G2-switch 1, G3-switch 2, G4, and G5 (see Figure 1). Select amino acid side chains are shown and numbered. The bound nucleotide (ppGpp) and two magnesium ions (blue spheres) are shown covered by simulated annealing omit map electron density contoured at 1.50 σ [42].

various Obg nucleotide complexes (discussed below). G5 includes loop residues 310–315 between β strand 17 and helix G.

Structural analysis of the Obg protein revealed two monomers in the active site in different nucleotide-bound conformations, an observation not appreciated until structural refinement was released from noncrystallographic symmetry restraints. After this was done, it became clear that monomer A was in its apo state and that monomer B was in a nucleotide-bound configuration. Although many GTP binding domains have only been observed in either GDP- or GTP-bound configurations, few have been observed in their apo state. Some of these include Era [32], the signal recognition particle (SRP) GTPase Ffh [33], and the translocation/protein elongation GTPase EF-G [34]. In all of these cases, including Obg, respective switch elements mediate contacts between the G protein and the conserved N-terminal or C-terminal domains, suggesting mechanisms that transduce the nucleotide-bound state of the G protein to the additional domain.

The second BsObg monomer was observed in a nucleotide-bound configuration (monomer B). BsObg was expressed and purified as full-length protein (1–428) from *E. coli*, subjected to preparative proteolysis to generate BsObg(1–342), and crystallized without addition of exogenous nucleotides, suggesting that nucleotide complexes observed for Obg arose through copurification from *E. coli* lysates (see Experimental Procedures). When refinement neared completion, density within the monomer B-P loop could be interpreted as GDP and two magnesium ions. However, when GDP and magnesium were added to the model, it became clear that the bound molecule was more extensive than GDP and that additional atoms emanated from the 3′-OH of the ribose. Since few modified nucleotides are found in high concentration in the cell, the nucleotide was interpreted and modeled as ppGpp, a nucleotide found in millimolar concentrations under starvation or stress (Figure 5) [35].

At least two possibilities could explain the occurrence of ppGpp in the active site. Either Obg exhibits specificity for this nucleotide in biology associated with bacterial stress response or it is an artifact of the starvation conditions encountered by *E. coli* upon growth and induction of Obg in cells grown in media devoid of required nutrients. Although no direct contacts are observed with the ppGpp 3′-diphosphate, full-length BsObg(1-428)p purified from *E. coli* included the C-terminal TGS domain that is shared with other bacterial stress response proteins, such as SpoT, the pppGpp hydrolase [7, 23]. If bacterial TGS domains confer binding specificity for pppGpp or ppGpp, a mechanism for BsObg interaction with these nucleotides could provide a direct link between bacterial Obg proteins and bacterial stress response pathways. To the best of our knowledge, this is the first reported structure of a GTPase in complex with ppGpp.

Structures for other nucleotide-bound forms of Obg were obtained by cocrystallization of Obg in millimolar concentrations of GTP, GDP, or GMPPCP. Diffraction-quality crystals were obtained in the presence of GDP and GMPPCP. Analysis of the GMPPCP crystals revealed a GDP-bound configuration, consistent with GMPPCP degradation. Diffraction-quality crystals of the GTP-Obg were not obtained. From this analysis, two observations were made. First, ppGpp was not completely displaced in monomer B by cocrystallization with exogenous nucleotide. Second, no significant conformational differences were observed between monomer A structures in apo or GDP-bound configurations (data not shown). The only differences observed between apo and GDP-bound states occurred in G5 (310–315), the GTPase motif that includes residues in direct contact with the guanine base.

The putative GTPase switch elements mediate interactions between the Obg fold and GTP binding domain, suggesting a possible feedback mechanism between the two domains in response to GTP/GDP binding (Figures 1,

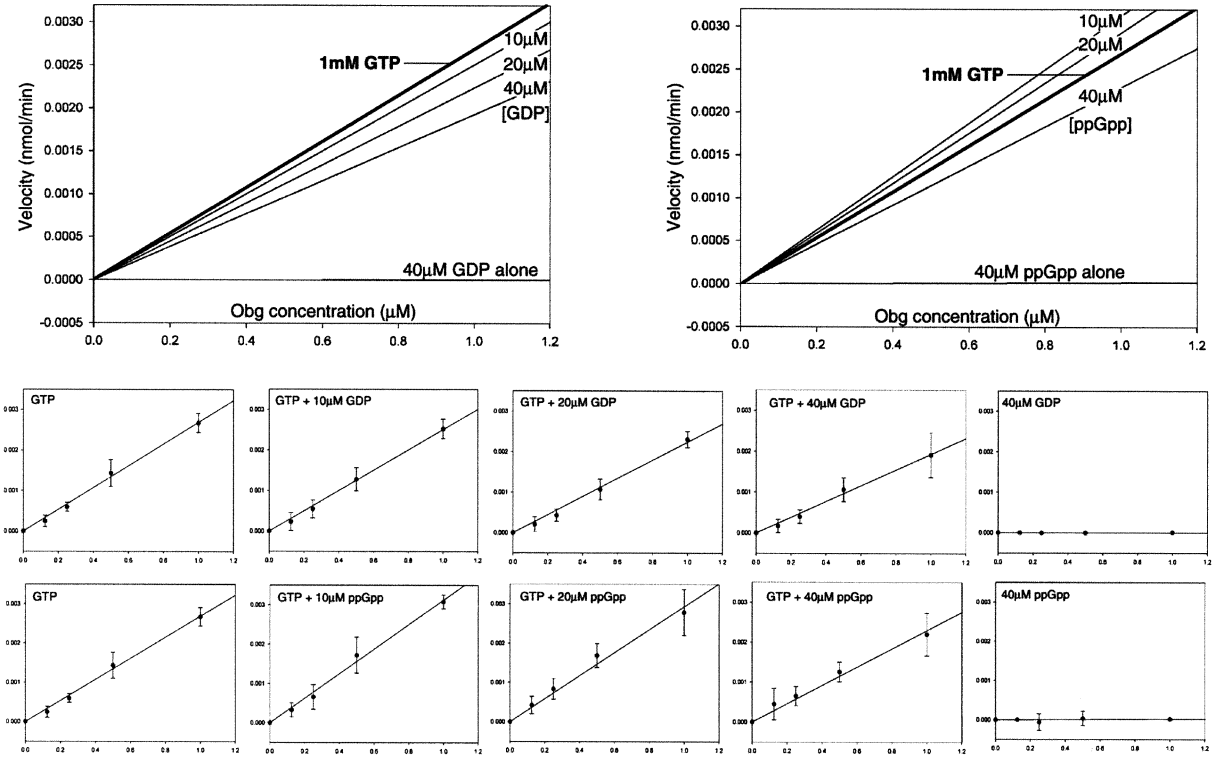

Figure 6. Effects of GDP and ppGpp on Obg-Catalyzed GTP hydrolysis

GTP hydrolysis was determined as a function of input protein for Obg(1–342)p. GTP hydrolysis rates (*y* axis in nanomoles per minute) are shown in both graphs as a function of Obg concentration (*x* axis in micromolar). GDP and ppGpp concentrations were increased from 0–40 μM to observe relative inhibition or stimulation of the respective GTP hydrolysis rates. Phosphate release from either GDP or ppGpp was determined in the absence of GTP in the reaction.

2, and 5). Analysis of Obg monomers in the asymmetric unit revealed slightly different orientations between the Obg fold and GTP binding domain, suggesting that switch element recognition of GTP- or GDP-bound configurations could trigger a conformational rearrangement between domains. However, lattice contacts were surmised as primarily responsible for the observed deviations, since no differences were observed between structures of monomer A in either apo or GDP-bound configurations between various crystals. This suggests that conformational changes associated with GDP binding were not sufficient to affect Obg domain movement.

Nucleotide Hydrolysis for Human and *B. subtilis* Obg Proteins

The structure of the *B. subtilis* Obg protein revealed ppGpp in the active site, prompting analysis of Obg proteins for GTP hydrolysis in the presence of various nucleotide substrates. Constructs encoding domains for human and *B. subtilis* proteins were made on the basis of our structural analysis of the Obg protein. HsObg(71–401)p and BsObg(1–342)p were expressed and purified (see Experimental Procedures). The human protein could only be expressed as soluble material in *E. coli* if the N-terminal 70 amino acids were removed, generating a fragment that included the conserved Obg fold and GTPase domain (Figure 1). Human Obg(71–401)p and *B. subtilis* Obg(1–342)p hydrolyzed GTP at a rate of 0.022 ± 0.005min^{-1} and 0.038 ± 0.007 min^{-1}, respectively. These rates are consistent with those previously reported for full-length *B. subtilis* Obg (0.006 min^{-1}) and *C. crescentus* CgtA (0.030 min^{-1}) [10, 18], suggesting that bacterial and human Obg enzymes encode similar mechanisms for GTP hydrolysis and rapid GTP/GDP exchange.

Previous reports revealed GDP inhibition of GTP hydrolysis for the *B. subtilis* Obg protein with a K_i of 1.7 μM [10]. To determine whether ppGpp represented a physiologically relevant factor during GTP hydrolysis, we compared Obg GTP hydrolysis rates in the presence of either GDP or ppGpp in assays using both Obg(1–342)p and the full-length protein (Figure 6). We could not detect differences between Obg(1–342)p and full-length protein in GTPase assays containing either GDP or ppGpp and have chosen to present GTP hydrolysis data for Obg(1–342)p, since this construct represents the structure described in this manuscript. The first GTPase assays conducted utilized 1 μM Obg and GTP at 40 μM, 80 μM, or 160 μM. In each of these sets, either GDP or ppGpp was added into the reaction mix at 0 μM, 2 μM, 4 μM, 8 μM, or 16 μM. Initial results indicated 2- to 4-fold rate decreases in the presence of GDP, confirming the previous observations that GDP inhibits Obg-mediated GTP hydrolysis. In contrast, ppGpp appeared to increase the rate of GTP hydrolysis by 2- to

5-fold over the same concentration range. We further characterized Obg-mediated GTP hydrolysis over four Obg concentrations (0.125 μM, 0.25 μM, 0.5 μM, and 1.0 μM), while keeping GTP concentrations constant at 1 mM, a concentration nearer to that observed in the cell. GDP or ppGpp was added to reactions at 0 μM, 10 μM, 20 μM, or 40 μM (Figure 6). These assays confirm GDP inhibition of Obg-mediated GTP hydrolysis, while suggesting stimulatory modes for ppGpp at lower concentrations and inhibitory modes at higher ppGpp concentrations. Commercial sources for pppGpp could not be identified, so it was not tested as a substrate in hydrolysis assays.

Although the K_i or K_m for ppGpp were not explicitly measured in these reactions, similar GDP and ppGpp concentrations elicited the same magnitude of response, albeit in opposite directions. These observations suggest that ppGpp has a binding constant for Obg in the micromolar range, as was previously observed for both GTP and GDP nucleotides. These data also suggest that differing cellular concentrations of ppGpp could directly influence Obg GTP hydrolysis rates. Although apparently not required for GDP inhibition or ppGpp stimulation, the *B. subtilis* Obg protein contains a C-terminal TGS domain, a domain that has been associated with the stringent response and ppGpp biology in the bacterial cell [7]. Although this domain is not conserved across all prokaryotic family members, conservation of the TGS domain in the *B. subtilis* Obg protein, when combined with our structural and biochemical observations, suggests that the *B. subtilis* Obg protein may have evolved to recognize ppGpp or pppGpp in response to changes in the cellular environment. Since ppGpp is not involved in eukaryotic responses to stress, its involvement in eukaryotic Obg function is not likely relevant.

Biological Implications

Structural and biochemical analyses of the Obg family of GTP binding proteins have revealed a unique architecture for the N-terminal glycine-rich domain, active sites in apo and ppGpp-bound states, a putative *B. subtilis* binding partner for the glycine-rich domain, similar intrinsic GTP hydrolysis rates for the human and bacterial Obg proteins, and a stimulatory and inhibitory role for ppGpp in *B. subtilis* Obg-mediated GTP hydrolysis. The structure provides the first detailed atomic characterization of conserved domains found within all Obg family members, suggesting functions for the glycine-rich domain (a binding platform) and how the Obg domain is coupled through the switch elements of the GTP binding domain. Similar interfaces are observed in other large G proteins, such as EF-TU, EF-G, and SRP GTP binding proteins, that function by modulating intramolecular domain rearrangements in response to GTP binding and hydrolysis. The structural data obtained for Obg should prove useful in further interpretation of genetic and biochemical experiments aimed at elucidating Obg-mediated pathways in the cell. The observation of ppGpp in the Obg active site P loop, a nucleotide copurified from bacterial lysates, suggests that bacterial Obg proteins may interact with this molecule in vivo, an interesting possibility, since Obg has long been associated with bacterial responses toward starvation or stress.

Obg proteins belong to a large group of diverse, but evolutionarily conserved, GTPases. The level of conservation suggests that Obg and other high-molecular weight GTP binding proteins in this class would be involved in core cellular functions, such as regulating or responding to transcription, translation, or stress response [4–6]. If Obg interacts with a large complex, such as the ribosome or polymerase complexes, the Obg domain could serve as a structural mimic for nucleic acid, conceptually similar to the mechanism proposed for EF-G mimicking of the EF-Tu tRNA complex. Interestingly, few surface residues are conserved within the Obg fold, indicating that the structure and shape of the platform are more important than residues presented on the surface. Although we subjected the domain to further structural and electrostatic analysis, the shape and properties observed for Obg did not reveal similarity to any standard nucleic acid structure.

Sequence analysis across multiple genomes has revealed the existence of several highly conserved multidomain GTP binding protein families. Since many of these families are poorly understood, we have initiated characterization and structure determination for several of these family members as part of the New York Structural Genomics Research Consortium (http://www.nysgrc.org). Our aim will be to elucidate structure-function relationships between GTP binding domains within these families and to assign structure and putative function to the equally conserved, but poorly understood, domains associated with them.

Experimental Procedures

Protein Expression and Purification

N-terminal His-tagged BsOBG(1–401)p was expressed from pET-28b in *E. coli* BL21(DE3)pLysS (Novagen), purified on Ni-NTA-agarose resin (Qiagen), and dialyzed (50 mM Tris-HCl [pH 8.0], 200 mM NaCl, and 2 mM β-mercaptoethanol) in the presence of thrombin (Sigma). Limited proteolysis was undertaken to identify domains within the protein, and a stable product roughly 5–7 kDa smaller than the full-length protein was identified. Preparative proteolysis produced sufficient quantities of the fragment for crystallization by digesting Obg with a 1:1000 w/w ratio of subtilisin to Obg. The proteolytic fragment was purified by size exclusion chromatography (Superdex 200) and anion exchange (MonoQ 10/10) (Pharmacia). Selenomethionyl protein was produced in DL41 DE3 cells [24]. The resulting protein was concentrated to ~13 mg/ml (20 mM Tris-HCl, 50 mM NaCl, and 1 mM DTT). Although the exact C terminus was not determined, crystallographic analysis of the domain revealed the C terminus to be at position 342, consistent with the increased mobility observed by SDS-PAGE for the proteolysis product.

Crystallization and Data Collection

BsObg crystals were grown by hanging drop vapor diffusion against a reservoir containing 7%–12% isopropanol, 0.1 M magnesium chloride, and 0.05 M sodium cacodylate (pH 6.5). These crystals belonged to space group $P2_12_12_1$ ($a = 59.55$ Å, $b = 104.98$ Å, $c = 124.07$ Å, and $\alpha = \beta = \gamma = 90°$). Cryopreserved crystals (30% sucrose) were screened on a laboratory copper Kα source (Rigaku RU 200, Osmic multilayer optics, and a Raxis-IV detector). Data sets on crystals obtained from various nucleotide cocrystallization experiments were collected at National Synchrotron Light Source (Brookhaven, NY) beamline X4A with an ADSC Quantum-4 detector. The four-wavelength MAD data set used to obtain experimental phases was collected at Structural Biology Center beamline 19-ID with undulator radiation [25]. Data was reduced with DENZO and

SCALEPACK (X4A), HKL2000 (APS 19-ID) [36], and the CCP4 suite [37].

Structure Determination and Refinement

Fifteen selenium sites were located and used to generate 2.8 Å phases with SOLVE [38]. Further phase refinement was accomplished with SHARP [39] and improved by density modification with SOLOMON [40]. The resulting maps were traced with O [41], and refinement was accomplished with CNS [42]. Manual rebuilding was followed by refinement at 2.6 Å, water placement, and ppGpp nucleotide modeling. The model, having excellent geometry, contained two monomers in the asymmetric unit, with monomer B in ppGpp-bound configuration, two magnesium ions, and amino acid residues 1–185 and 195–342. Monomer A contained amino acid residues 1–342, no ligand, or discernable magnesium ions. See Table 1 for further refinement details.

Structural similarities were calculated with DALI [26]. The Obg GTP binding domain shares similarity to ADP-ribosylation factor 1 (hArf1, Arf1, mArf1) (Protein Data Bank code 1hur, 3.2 Å rmsd over 141 amino acids, with 20% sequence identity [ID]), elongation factor (EF-TU) (Protein Data Bank code 1efc, 3.1 Å rmsd over 141 amino acids, with 18% ID), transforming protein p21H-RAS-1 (Protein Data Bank code 1ctq, 3.3 Å rmsd over 138 amino acids, with 15% ID), elongation factor G (EF-G) (Protein Data Bank code 1dar, 3.4 Å rmsd over 143 amino acids, with 23% ID), GTP binding protein Ran (TC4) (Protein Data Bank code 1byu, 2.9 Å rmsd over 139 amino acids, with 17% ID), guanine nucleotide binding protein α-1 subunit (Gi-α-1) (Protein Data Bank code 1cip, 3.4 Å rmsd over 140 amino acids, with 15% ID), and the GTP binding protein Era (Protein Data Bank code 1ega, 3.6 Å rmsd over 133 amino acids, with 20% ID).

GTPase Assay, Lysate Affinity Assay, Yeast Plasmids, and Strains

B. subtilis Obg was cloned into pET28b to generate N-terminal His_6 fusions and into pGEX-2T to obtain C-terminal fusions with glutathione S-transferase. Both His_6 and GST fusions were linked to Obg by a thrombin cleavage sequence. Several domains were fused to GST, including full-length (1–401), N-terminal (1–161), and C-terminal (161–401) residues. *Bacillus subtilis* strain JH642 was grown by fermentation, harvested during log phase (0.4 OD_{600}), centrifuged, resuspended, and lysed by sonication in 50 mM Tris (pH 7.5), 150 mM NaCl, 1 mM PMSF, and 0.1% IGEPAL. The lysate was centrifuged in two cycles: first at 5,000 $\times$ g for 30 min and then at 10,000 $\times$ g for 1 hr. The resulting supernatant, containing 18 mg/ml protein, as measured by Bradford analysis, was dialyzed overnight against 50 mM NaCl, 50 mM Tris (pH 7.5), and 1 mM BME. Fifty-four milligrams of lysate (containing 50, 150, or 600 mM NaCl) was mixed with 100 μg of respective GST-Obg protein (0.18% Obg protein-lysate) and incubated for 1 hr at 4°C. After incubation, the protein-lysate mix was incubated with 50 μl glutathione Sepharose resin for 15 min at 4°C. The resin was washed with 3 $\times$ 1 ml of buffer containing 50 mM NaCl, 50 mM Tris (pH 7.5), and 1 mM BME. Protein was liberated from the beads with buffer containing 50 mM reduced glutathione (to release the GST-Obg fusion and respective binding proteins) or 5 units bovine thrombin (Sigma) to release the Obg domain and respective binding proteins (1 hr at 4°C). Samples were analyzed by SDS-PAGE. TasA was identified by N-terminal sequencing.

Human Obg was cloned from a human testes library and cloned into pET28b for expression (Novagen). Protein expressed from *E. coli* was obtained by previously described methods for BsObg. GTPase assays for human and bacterial Obg were conducted with 2 μM enzyme in buffer containing 10 mM $MgCl_2$, 1 mM GTP, 100 mM Tris (pH 8.0), 100 mM NaCl, and 0.1% Tween. Time points were taken up to 18 hr, and released phosphate was measured by a malachite green phosphate assay (Cytoskeleton). Guanasine 5′-, 3′-diphosphate (ppGpp) was purchased from Tri-link Biotech. Assays for GDP and ppGpp inhibition of GTP hydrolysis were conducted with both full-length (1–401) and truncated (1–342) *B. subtilis* Obg protein. GTP hydrolysis rates were determined as a function of input protein. One millimolar GTP was utilized in reactions in the presence of 0 μM, 10 μM, 20 μM, or 40 μM ppGpp or GDP. Obg-mediated ppGpp or GDP hydrolysis was also determined by removing GTP from the reaction mixtures. All reaction conditions were conducted in the absence of enzyme to assess respective background phosphate concentrations of the input nucleotides. Reaction buffer conditions were identical to those described above, except that the reactions were incubated for 16 hr. Released phosphate was measured with Biomol Green (Biomol Research Labs). Purified BsObg(1–161)p was used as a control and did not show GTPase activity beyond background.

Acknowledgments

We thank the staffs of beamline X4A and 19-ID at the DOE facilities at the National Synchrotron Light Source and Advanced Photon Source, respectively. We thank Ryan Kniewel for critical reading of the manuscript. Beamline X4A is supported by the Howard Hughes Medical Institute. This work was supported by a Young Investigator award made to C.D.L from the Arnold and Mabel Beckman Foundation and by NIH structural genomics pilot center grant 1P50 GM62529.

Received: June 7, 2002
Revised: July 31, 2002
Accepted: August 29, 2002

References

1. Bourne, H.R., Sanders, D.A., and McCormick, F. (1990). The GTPase superfamily: a conserved switch for diverse cell functions. Nature *348*, 125–132.
2. Bourne, H.R., Sanders, D.A., and McCormick, F. (1991). The GTPase superfamily: conserved structure and molecular mechanism. Nature *349*, 117–127.
3. Geyer, M., and Wittinghofer, A. (1997). GEFs, GAPs, GDIs and effectors: taking a closer (3D) look at the regulation of Ras-related GTP-binding proteins. Curr. Opin. Struct. Biol. *7*, 786–792.
4. Mittenhuber, G. (2001a). Comparative genomics of prokaryotic GTP-binding proteins (the Era, Obg, EngA, ThdF (TrmE), YchF and YihA families) and their relationship to eukaryotic GTP-binding proteins (the DRG, ARF, RAB, RAN, RAS and RHO families). J. Mol. Microbiol. Biotechnol. *3*, 21–35.
5. Caldon, C.E., Yoong, P., and March, P.E. (2001). Evolution of a molecular switch: universal bacterial GTPases regulate ribosome function. Mol. Microbiol. *41*, 289–297.
6. Leipe, D.D., Wolf, Y.I., Koonin, E.V., and Aravind, L. (2002). Classification and evolution of P-loop GTPases and related ATPases. J. Mol. Biol. *317*, 41–72.
7. Wolf, Y.I., Aravind, L., Grishin, N.V., and Koonin, E.V. (1999). Evolution of aminoacyl-tRNA synthetases—analysis of unique domain architectures and phylogenetic trees reveals a complex history of horizontal gene transfer events. Genome Res. *9*, 689–710.
8. Sonenshein, A.L. (2000). Control of sporulation initiation in Bacillus subtilis. Curr. Opin. Microbiol. *3*, 561–566.
9. Kok, J., Trach, K.A., and Hoch, J.A. (1994). Effects on Bacillus subtilis of a conditional lethal mutation in the essential GTP-binding protein Obg. J. Bacteriol. *176*, 7155–7160.
10. Welsh, K.M., Trach, K.A., Folger, C., and Hoch, J.A. (1994). Biochemical characterization of the essential GTP-binding protein Obg of Bacillus subtilis. J. Bacteriol. *176*, 7161–7168.
11. Vidwans, S.J., Ireton, K., and Grossman, A.D. (1995). Possible role for the essential GTP-binding protein Obg in regulating the initiation of sporulation in Bacillus subtilis. J. Bacteriol. *177*, 3308–3311.
12. Trach, K., and Hoch, J.A. (1989). The Bacillus subtilis spo0B stage 0 sporulation operon encodes an essential GTP-binding protein. J. Bacteriol. *171*, 1362–1371.
13. Scott, J.M., and Haldenwang, W.G. (1999). Obg, an essential GTP binding protein of Bacillus subtilis, is necessary for stress activation of transcription factor sigma(B). J. Bacteriol. *181*, 4653–4660.
14. Scott, J.M., Ju, J., Mitchell, T., and Haldenwang, W.G. (2000). The Bacillus subtilis GTP binding protein obg and regulators of

the sigma(B) stress response transcription factor cofractionate with ribosomes. J. Bacteriol. *182*, 2771–2777.
15. Okamoto, S., Itoh, M., and Ochi, K. (1997). Molecular cloning and characterization of the obg gene of Streptomyces griseus in relation to the onset of morphological differentiation. J. Bacteriol. *179*, 170–179.
16. Okamoto, S., and Ochi, K. (1998). An essential GTP-binding protein functions as a regulator for differentiation in Streptomyces coelicolor. Mol. Microbiol. *30*, 107–119.
17. Maddock, J., Bhatt, A., Koch, M., and Skidmore, J. (1997). Identification of an essential Caulobacter crescentus gene encoding a member of the Obg family of GTP-binding proteins. J. Bacteriol. *179*, 6426–6431.
18. Lin, B., Covalle, K.L., and Maddock, J.R. (1999). The Caulobacter crescentus CgtA protein displays unusual guanine nucleotide binding and exchange properties. J. Bacteriol. *181*, 5825–5832.
19. Lin, B., and Maddock, J.R. (2000). The N-terminal domain of the Caulobacter crescentus CgtA protein does not function as a guanine nucleotide exchange factor. FEBS Lett. *484*, 29–32.
20. Lin, B., Skidmore, J.M., Bhatt, A., Pfeffer, S.M., Pawloski, L., and Maddock, J.R. (2001). Alanine scan mutagenesis of the switch I domain of the Caulobacter crescentus CgtA protein reveals critical amino acids required for in vivo function. Mol. Microbiol. *39*, 924–934.
21. Kobayashi, G., Moriya, S., and Wada, C. (2001). Deficiency of essential GTP-binding protein ObgE in Escherichia coli inhibits chromosome partition. Mol. Microbiol. *41*, 1037–1051.
22. Slominska, M., Konopa, G., Wegrzyn, G., and Czyz, A. (2002). Impaired chromosome partitioning and synchronization of DNA replication initiation in an insertional mutant in the Vibrio harveyi cgtA gene coding for a common GTP-binding protein. Biochem. J. *362*, 579–584.
23. Mittenhuber, G. (2001b). Comparative genomics and evolution of genes encoding bacterial (p)ppGpp synthetases/hydrolases (the Rel, RelA and SpoT proteins). J. Mol. Microbiol. Biotechnol. *3*, 585–600.
24. Hendrickson, W.A., Horton, J.R., and LeMaster, D.M. (1990). Selenomethionyl proteins produced for analysis by multiwavelength anomalous diffraction (MAD): a vehicle for direct determination of three-dimensional structure. EMBO J. *9*, 1665–1672.
25. Hendrickson, W.A. (1991). Determination of macromolecular structures from anomalous diffraction of synchrotron radiation. Science *254*, 51–58.
26. Holm, L., and Sander, C. (1993). Protein structure comparison by alignment of distant matrices. J. Mol. Biol. *233*, 123–138.
27. Nicholls, A., Sharp, K.A., and Honig, B. (1991). Protein folding and association: insights from the interfacial and thermodynamic properties of hydrocarbons. Proteins Struct. Funct. Genet. *11*, 281–296.
28. Kramer, R.Z., Bella, J., Mayville, P., Brodsky, B., and Berman, H.M. (1999). Sequence dependent conformational variations of collagen triple-helical structure. Nat. Struct. Biol. *6*, 454–457.
29. Stover, A.G., and Driks, A. (1999a). Secretion, localization, and antibacterial activity of TasA, a Bacillus subtilis spore-associated protein. J. Bacteriol. *181*, 1664–1672.
30. Stover, A.G., and Driks, A. (1999b). Regulation of synthesis of the Bacillus subtilis transition-phase, spore-associated antibacterial protein TasA. J. Bacteriol. *181*, 5476–5481.
31. Serrano, M., Zilhao, R., Ricca, E., Ozin, A.J., Moran, C.P., Jr., and Henriques, A.O. (1999). A Bacillus subtilis secreted protein with a role in endospore coat assembly and function. J. Bacteriol. *181*, 3632–3643.
32. Chen, X., Court, D.L., and Ji, X. (1999). Crystal structure of ERA: a GTPase-dependent cell cycle regulator containing an RNA binding motif. Proc. Natl. Acad. Sci. USA *96*, 8396–8401.
33. Montoya, G., Svensson, C., Luirink, J., and Sinning, I. (1997). Crystal structure of the NG domain from the signal-recognition particle receptor FtsY. Nature *385*, 365–368.
34. Ævarsson, A., Brazhnikov, E., Garber, M., Zheltonosova, J., Chirgadze, Y., al-Karadaghi, S., Svensson, L.A., and Liljas, A. (1994). Three-dimensional structure of the ribosomal translocase: elongation factor G from Thermus thermophilus. EMBO J. *13*, 3669–3677.
35. Chatterji, D., and Ojha, A.K. (2001). Revisiting the stringent response, ppGpp and starvation signaling. Curr. Opin. Microbiol. *4*, 160–165.
36. Otwinowski, Z., and Minor, W. (1997). Processing of X-ray diffraction data collected in oscillation mode. Methods Enzymol. *276*, 307–326.
37. Collaborative Computational Project 4. (1994). The CCP4 suite: programs for protein crystallography. Acta Crystallogr. D Biol. Crystallogr. *50*, 760–763.
38. Terwilliger, T.C., and Berendzen, J. (1999). Automated MAD and MIR structure solution. Acta Crystallogr. D Biol. Crystallogr. *55*, 849–861.
39. de La Fortelle, E., and Bricogne, G. (1997). Maximum-likelihood heavy-atom parameter refinement for multiple isomorphous replacement and multiwavelength anomalous diffraction methods. Methods Enzymol. *276*, 472–494.
40. Abrahams, J.P., and Leslie, A.G.W. (1996). Methods used in the structure determination of bovine mitochondrial F1 ATPase. Acta Crystallogr. D Biol. Crystallogr. *52*, 30–42.
41. Jones, T.A., Zou, J.Y., Cowan, S.W., and Kjeldgaard, M. (1991). Improved methods for building protein models in electron density maps and the location of errors in these models. Acta Crystallogr. A *47*, 110–118.
42. Brunger, A.T., Adams, P.D., Clore, G.M., DeLano, W.L., Gros, P., Grosse-Kunstleve, R.W., Jiang, J.S., Kuszewski, J., Nilges, M., Pannu, N.S., et al. (1998). Crystallography and NMR system: a new software suite for macromolecular structure determination. Acta Crystallogr. D Biol. Crystallogr. *54*, 905–921.
43. Evans, S.V. (1993). SETOR: hardware-lighted three-dimensional solid model representations of macromolecules. J. Mol. Graph. *11*, 134–138.

Accession Numbers

Coordinates and structure factors are deposited in the Protein Data Bank under accession number 1LNZ.